Hindawi
Journal of Chemistry
Volume 2023, Article ID 9843284, 1 page
https://doi.org/10.1155/2023/9843284

Retraction

Retracted: Study on the Color Genesis of South Red Agate and the Geological Characteristics of the Siliceous Gravel Layer

Journal of Chemistry

Received 15 August 2023; Accepted 15 August 2023; Published 16 August 2023

This article has been retracted by Hindawi following an investigation undertaken by the publisher [1]. This investigation has uncovered evidence of one or more of the following indicators of systematic manipulation of the publication process:

(1) Discrepancies in scope

(2) Discrepancies in the description of the research reported

(3) Discrepancies between the availability of data and the research described

(4) Inappropriate citations

(5) Incoherent, meaningless and/or irrelevant content included in the article

(6) Peer-review manipulation

The presence of these indicators undermines our confidence in the integrity of the article's content and we cannot, therefore, vouch for its reliability. Please note that this notice is intended solely to alert readers that the content of this article is unreliable. We have not investigated whether authors were aware of or involved in the systematic manipulation of the publication process.

Wiley and Hindawi regrets that the usual quality checks did not identify these issues before publication and have since put additional measures in place to safeguard research integrity.

We wish to credit our own Research Integrity and Research Publishing teams and anonymous and named external researchers and research integrity experts for contributing to this investigation.

The corresponding author, as the representative of all authors, has been given the opportunity to register their agreement or disagreement to this retraction. We have kept a record of any response received.

References

[1] K. Li and Y. Yuan, "Study on the Color Genesis of South Red Agate and the Geological Characteristics of the Siliceous Gravel Layer," *Journal of Chemistry*, vol. 2022, Article ID 9157753, 7 pages, 2022.

Hindawi
Journal of Chemistry
Volume 2022, Article ID 9157753, 7 pages
https://doi.org/10.1155/2022/9157753

Research Article

Study on the Color Genesis of South Red Agate and the Geological Characteristics of the Siliceous Gravel Layer

Kongliang Li[1] **and Ye Yuan**[2]

[1]*Anhui Technical College of Industry and Economy, Hefei, Anhui 230051, China*
[2]*China University of Geosciences (Beijing), Beijing 430074, China*

Correspondence should be addressed to Kongliang Li; 11233311@stu.wxic.edu.cn

Received 20 April 2022; Revised 19 May 2022; Accepted 26 May 2022; Published 11 June 2022

Academic Editor: K. K. Aruna

The aim of the study was to explore the gem mineralogical characteristics of southern red agate and then analyze its structural characteristics and color causes. The mineral composition, structure, and chromogenic minerals of Nanhong agate were tested by a conventional gemmological test and observed under the microscope, infrared spectrum, and microlaser Raman spectrum. It is found that the color of southern red agate samples is mainly dark red or orange red, and colorless, white or yellow bands can be seen in some samples; the relative density is in the range of 2.59~2.65. The matrix structure of the sample is mainly long fiber and short fiber, and some of them are fine-grained and crystalline plasmid. There are concentric ring-banded structures, and some horizontal banded and vein structures can also be seen. The analysis and test results show that the south red agate has a typical radial fiber structure, and the main chemical component is SiO_2; Under the orthogonal polarizing microscope, a large number of round reddish brown mineral inclusions with banded distribution can be seen, the spot-colored mineral is iron oxide hematite, and calcite of the late hydrothermal origin can be seen in the cracks. In addition, the study shows that the formation of south red agate is multistage and the formation of hematite inclusions is also multistage.

1. Introduction

The application history of southern red agate can be traced back to the period of Hongshan culture. It has been used by royal families and nobles as early as the northern and southern dynasties. From the Ming and Qing dynasties to now, high-quality Nanhong agate has always been an important material for jewelry. It is one of the jade varieties with a long history in China. Nanhong agate is a unique species in China. It is named for its main mining area in Baoshan, Yunnan, in history. However, it is not only produced in Yunnan that it is called Nanhong agate [1]. In a broad sense, southern red refers to the general name of red agate with bright colors produced in southwest China. Its three major producing areas are Baoshan southern red in Yunnan (southern Yunnan red), Liangshan southern red in Sichuan (southern Sichuan red), and Diebu southern red in Gansu (southern Gansu red). The common Nanhong agate in the market is mainly produced in Baoshan, Yunnan, and Liangshan, Sichuan. Sichuan Nanhong is a variety of Nanhong that has been developed in large quantities in recent years. It is produced in Meigu area of Liangshan Prefecture, Sichuan province. It was discovered and mined in 2009 [2]. The discovery of Sichuan Nanhong has greatly alleviated the problems of low output, many grain cracks, and exhausted mining of Baoshan Nanhong and led to a new "Nanhong fever." For a time, the price of Nanhong agate soared and became the darling of the collection industry again. Nowadays, the price of southern red agate has soared all the way, while similar Mongolian red agate, Xinjiang red agate, and African red agate do not have such a high price. The gemstone mineralogical characteristics and chromogenic mechanism of southern red agate need to be studied. What is the difference between southern red agate and red agate from other producing areas and how to distinguish it from imitations in the market are worthy of our discussion

[3]. The research on the south red agate will help people better understand south red agate and play a certain role in the identification work and the prospecting work of the south red agate.

2. Literature Review

Redlisiak et al. said that south red agate, often referred to as "south red," is a general term for a natural red agate that is mainly red and moist and thick in appearance produced in southwest China in recent years [4]. Kondratyeva et al. said that in China, south red agate has a long application history and its earliest use can be traced back to the period of Hongshan culture [5]. Lu et al. said that the earliest surviving south red product is the south red shell coin unearthed at the Jinsha site in Chengdu, which follows the tradition of using shell coins by the ancestors of Sanxingdui [1]. Zheng– Sheng et al. said that in the tombs of the nobles of the ancient Dian state during the Warring States period, many strings of Nanhong agate and two Nanhong agate carvings of beetles and cow heads were also unearthed [6]. Wang et al. found through investigation that until the Ming and Qing dynasties, Nanhong agate once became a substitute for red coral and was known as one of the "seven treasures of Buddhism." It has an extremely special position in Tibetan Buddhism and is widely used in Buddha beads and bracelets [7]. Zhu et al. said that during the Qianlong period of the Qing dynasty, Nanhong agate won the favor of the royal family, so a large number of Nanhong agates were paid as tribute to the court. So far, it reached its first heyday. The beautiful color carvings of Nanhong agate such as "double fish dragon flower arrangement" and "bat peach tree flower arrangement" in the Qing dynasty are still collected in the Palace Museum [8]. Golovanova and Pitieva believed that in terms of metallogenic environment, Chinese agate often occurs in volcanic rock series, and its mineralization is mainly magmatic hydrothermal alteration and hydrothermal filling. And common agate deposits occur in basalt formation, neutral volcanic rock formation, acid TUFF formation, and residual slope alluvial clastic formation, which provides suggestions for the prospecting direction of agate [9]. Huang et al. carried out a field investigation in the mining area of Nanhong agate and performed a specific analysis on the metallogenic environment. Among them, the Nanhong agate deposit in Liangshan, Sichuan province, belongs to the magmatic hydrothermal deposit, which takes the hydrothermal formed by basalt magmatic eruption as the material source. The metallogenic process mainly includes primary and secondary ore. At present, the mined deposits are sedimentary conglomerate deposits [10]. Wang et al. believe that the deposit type of Nanhong agate in Baoshan, Yunnan, belongs to the low-temperature hydrothermal colloidal deposit formed in the later stage of magma, which is mainly produced in the Quaternary strata and often filled in the almond pores and fractures of basalt [11]. Combined with the study of metallogenic environment and basic gem mineralogical characteristics, Krasilnikov et al. also performed a specific analysis on the color genesis of south red agate. They believed that south red agate is mainly colored by inclusions [12].

3. Method

3.1. South Red Agate Samples Are Selected for Testing. A total of 8 samples of Nanhong agate (hereinafter referred to as "combined material") used in this paper are produced in the mine mouth of Lianhe Township, Meigu County, Liangshan Prefecture, Sichuan Province, and provided by an Auction Co., Ltd. The samples are numbered from L-101 to L-108. Samples L-101, L-102, L-105, and L-107 have epidermis. The part of sample L-107 is crystalline white quartz particles, and the other three are southern red agate with uniform appearance [13]. The basic characteristics are shown in Table 1.

Through the observation of the specimen, it can be seen that the color of the "combined material" of south red agate is mainly red with an orange or pink hue. The "cherry red" (also known as "water red") in the color classification of south red agate comes from the "combined material". Transparency is translucent-transparent. In addition, some white areas appear in sample L-106 and the white part is slightly transparent and opaque. The south red agate combined material has a conch fracture, which is oily and shiny because it contains cryptocrystalline-microcrystalline aggregate. It can be seen to the naked eye that densely distributed red granular mineral inclusions are distributed in the whole sample. The red mineral runs through almost the whole sample. For samples with bands, red granular inclusions gather along the bands, while the distribution of red minerals is relatively sparse at non-bands. The diameter of red mineral particles in most samples is between 10 and 80 μm, and the naked eye needs to observe with the help of transmitted light. In sample L-104, the diameter of some red mineral particles reaches $100 \sim 200\,\mu$m, while the diameter of red minerals in samples L-107 and L-108 even reaches $400\,\mu$m, which is clearly visible to the naked eye under natural light [14]. In addition, some areas of sample L-107 are crystalline white quartz. At the transition between quartz and agate, some positions are red. Different from the surrounding red granular inclusions, the red part cannot distinguish particles and is cryptocrystalline. It is not difficult to find that the color of the "combined material" of south red agate is closely related to the distribution of red mineral inclusions. In areas where red inclusions are densely distributed, the thicker the red, the thinner the particles are distributed, and the lighter the color or even become colorless.

3.2. Geological Characteristics of the Siliceous Gravel Layer

3.2.1. Profile Description. The tectonic location in the area is the Yangtze carbonate platform tectonic area of the upper Yangtze block, which mainly exposes Cambrian-Triassic strata, and the structural features are mainly NE trending folds and faults. The elevation of this section is 1125 m, the highest part of the mountain top is 1500 m, and the average slope angle is 37°. The gravel layer is located at the gentle slope of the depression. The exposed width of the gravel layer is about 20 m, the thickness is 10 m, and the exposed length is 30 m. The lower part is damaged by denudation and highway construction, and its exposed characteristics are unknown. The material composition of each layer of the gravel layer is mainly gravel, and only the 4th and 7th layers

Table 1: Basic characteristics of "combined material".

Sample number	Size (cm)	Color	Mass (g)	Relative density
L-101	$4.51 \times 4.28 \times 2.61$	The center is red, the band is red or orange red, and the band gap is orange yellow or colorless	52.5	2.6
L-102	$3.37 \times 2.07 \times 1.16$	Red	9.0	2.6
L-103	$3.31 \times 1.73 \times 1.32$	Red	10.9	2.6
L-104	$3.22 \times 4.28 \times 2.61$	The strip is red, and other areas are colorless or light red	18.0	2.7
L-105	$3.81 \times 2.70 \times 12.61$	Red	16.9	2.6
L-106	$2.91 \times 2.59 \times 1.41$	Red, white appears in some areas, and there is no obvious boundary with red	16.9	2.6
L-107	$4.35 \times 3.44 \times 1.61$	Red	31.2	2.6
L-108	$2.80 \times 2.21 \times 1.86$	Red	11.3	2.6

are gravelly sand clay layers. The overall gravel diameter is relatively coarse, mostly 2~8 cm. The gravels are mostly angular and basically not rounded. The composition of gravel is relatively single, which is basically composed of dolomite [15]. The boundary between layers is obvious. According to the characteristics of the gravel combination and gravel diameter change, it is divided into 9 layers from bottom to top. Generally speaking, the larger the gravel diameter of the gravel layer, the stronger its hydrodynamic force. According to the gravel diameter, the gravel layer in the survey area is divided into four sedimentary cycles and the circular column diagram is established. Cycle 1 is layer 2–4. The gravel diameter of the lower part is 10 cm, and the average gravel diameter is 2 cm in the upward transition. It has obvious binary structure characteristics of coarse at the bottom and fine at the top, and the sand clay and gravel of layer 4 are mixed and accumulated, showing the characteristics of sharp weakening of water flow power. Cycle 2 is the fifth layer, with a gravel diameter of 8 cm and upward to 2 cm. Cycle 3 is the 8th layer, which is distributed in the lenticular shape, the lower part is supported gravel, basically without the matrix, and the upper part is gravelly sand clay layer. Cycle 4 is 9–10 layers, with a gravel diameter of 12 cm in the lower part and 5 cm in the upper part, with obvious changes. The gravel diameter of each cycle decreases from bottom to top, reflecting the gradual reduction of hydrodynamic force of each cycle [16]. The gravels in the gravel layer are characterized by poor roundness and single gravel composition, which reflect that the material source is close. The gravel layer has a certain sorting property, and there is no matrix in the layer, which reflects that its deposition process has a certain duration, which is speculated to be the characteristics of intermountain flood alluvial deposition.

3.2.2. Gravel Particle Size Characteristics. The particle size analysis of the gravel layer adopts a manual direct measurement method. According to the horizon direction of the gravel layer, samples shall be taken from bottom to top in the vertical bedding direction. Each layer shall be sampled with a 50 cm × 50 cm grid, and the length of the gravel axis in the grid shall be counted. By measuring 9 groups of samples in the gravel layer, the gravel in the gravel layer is mostly concentrated in 3~12 cm, accounting for more than 70%. Only sample 6 is mainly composed of fine particles such as sand and clay, and the gravel content is 42%. The particle size parameters are calculated according to the Folk–Ward formula, as shown in Table 2, and the results are shown in Table 3. The overall average particle size of the gravel layer is −4.26 (19 mm). The average particle size of sample 13 decreased gradually. The average particle size of samples 4–6 decreased from −5.7 to −1.62, indicating that the water flow velocity decreased gradually.

The average particle size of samples 1, 2, 4, 5, 8, and 9 is $\varphi < -4$ (> 16 mm), and the sorting coefficient is between 1 and 2, indicating that its sorting property is medium. While the field outcrop of the corresponding layer shows that each layer is supported by particles, and there is little matrix deposition such as clay and sand. The average particle size ϕ in samples 3, 6, and 7 is–1~–4 (2 ~ 16 mm), and its particle size is relatively small. The sorting coefficient is between 2 and 4, and the sorting property is poor. The absolute values of skewness are >10, and there are two asymmetric particle size peaks and the sorting property is poor [17]. Combined with the field outcrop identification, the fourth layer corresponding to sample 3 is the grayish yellow coarse gravel layer containing sand and clay and the fine particles such as sand and clay are significantly increased. The frequency accumulation curve shows that the sediment has two obvious peaks, as shown in Figure 1.

4. Results and Analysis

4.1. Structural Characteristics of South Red Agate. Nanhong agate particles are closely combined and have a near aphanitic structure. Its structural characteristics cannot be accurately observed under a 10× magnifying glass. In order to observe the structural characteristics more clearly, the raw stone samples are converted into mineral flakes and observed under a polarizing microscope. The samples under an orthogonal polarizer have a typical radial fiber structure. Due to multiple crystals in the same structural layer, the crystals are perpendicular to the base and extend synchronously to the opposite side since the microcrystalline bud, resulting in the radioactive growth of the crystals from a point or a mineral edge. Due to the poor fluidity of SiO_2 colloid, the crystal can only grow into fine fibrous crystals with radial structure. The color of southern red agate is related to the red dot minerals that are roughly banded and densely distributed. Under a 1000× microscope, it is a small

Table 2: Particle size parameter formula.

Name	Folk and Ward
Median	$M_{d\varphi} = \varphi_{50}$
Average particle size	$M_Z = (\varphi 16 + \varphi 50 + \varphi 84/3)$
Sorting	$\sigma_1 = (\varphi 84 - \phi 16/4) + (\phi 95 - \phi 5/6.6)$
Skewness	$SK_1 = (\varphi 16 + \varphi 84 - 2\varphi 50/2(\varphi 84 - \varphi 16)) + (\varphi 5 + \varphi 95 - 2\varphi 50/2(\varphi 95 - \varphi 5))$
Kurtosis	$K_G = (\varphi 95 - \varphi 5/(2.44(\varphi 75 - \varphi 25)))$

Table 3: Gravel composition and particle size parameters.

Sample number	Layer number	Average particle size (φ)	Sorting coefficient (σ_1)	Skewness (SK_1)	Kurtosis (K_G)
1	2	−4.97	1.6	−2.19	0.73
2	3	−4.71	1.63	5.47	1.24
3	4	−3.51	2.4	11.47	0.59
4	5	−5.7	1.14	3.46	0.75
5	6	−4.21	1.03	1.25	1.21
6	7	−1.42	2.17	−20.34	0.71
7	8	−3.1	2.23	14.26	0.51
8	9	−5.7	1.35	2.37	0.74
9	10	−4.9	1.37	2.33	0.71

nearly spherical reddish brown chromogenic mineral with incomplete crystal morphology and the existence of nearly hexagonal particles. Fourier near infrared spectroscopy was used to test three bead samples with good surface polishing in different areas [18]. Test conditions: room temperature, reflection method, the measurement range is set to 400~2000 cm^{-1}, the resolution is 4 cm^{-1}, and 30 scans. The comparison results of infrared absorption spectra are shown in Figure 2.

In Figure 2, south red agate has five obvious absorption peaks, namely, 496, 541, 783, 1099, and 1195 cm^{-1}, that is, the main mineral composition of south red agate is α-quartz. Due to the fine structure of Nanhong agate, it is difficult to determine the species of some minerals using the microscope and laser Raman analysis technology is often used for qualitative and quantitative analysis of small areas of rock and mineral analysis. Therefore, Raman spectroscopy is used to further determine the species of nearly spherical chromogenic minerals. The spectrum obtained from the laser Raman test of reddish brown punctate minerals with banded and dense distribution seen by the naked eye is shown in Figure 3.

The test conditions are as follows: argon ion laser 532 nm; the test range is 100~3000 cm^{-1}; scanning 3 times, laser scanning spot 1 μm. Figure 4 shows the Raman spectrum of south red agate chromogenic minerals.

According to Figure 4, the test samples have 228.93, 248.44, 295.48, 413.56, 467.33, 501, 613.84, and 1320.50 cm^{-1} obvious scattering peaks. The Raman spectra of reddish brown near spherical minerals in southern red agate are very similar; the scattering peaks around 467 cm^{-1} and 1320 cm^{-1} are strong, and the other peaks are mainly distributed between 130 and 620 cm^{-1}. Comparing the test data with the Raman data of minerals in the RRUFF database, the absorption of scattering peaks near 130, 210, and 468 cm^{-1} is α-quartz. The absorption mineral of the scattering peak near 225, 245, 294, 410, 499, 501, and 61ll cm^{-1} is hematite, that is,

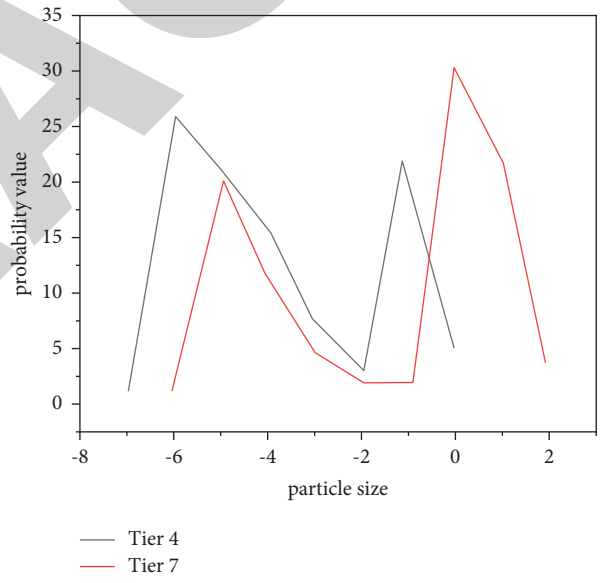

Figure 1: Grain size frequency curve of sediments in layers 4 and 7.

the red nearly spherical mineral inclusions distributed in strips are iron oxide hematite, the absorption peak at 501 cm^{-1} is the strong scattering peak of SiO_2, 1320 cm^{-1} in the form of clinopyroxene, and the absorption is the characteristic absorption peak spectrum of calcite [19]. The results of Raman scattering peaks show that the main mineral of south red agate is α-quartz, the nearly spherical chromogenic mineral distributed in a strip is iron oxide hematite, and the fissure is filled with calcite and other minerals of the late hydrothermal origin.

4.2. Discussion on Color Causes and Influencing Factors of South Red Agate. Through the comprehensive test and analysis of south red agate and yellow and white comparison samples, it can be determined that the main chromogenic

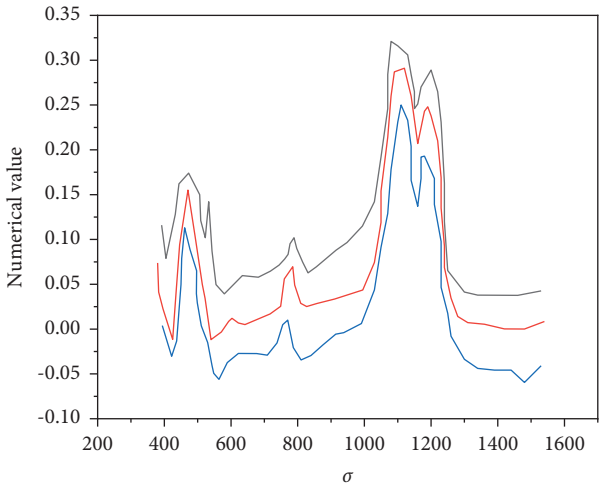

Figure 2: Comparison of infrared absorption spectra of south red agate.

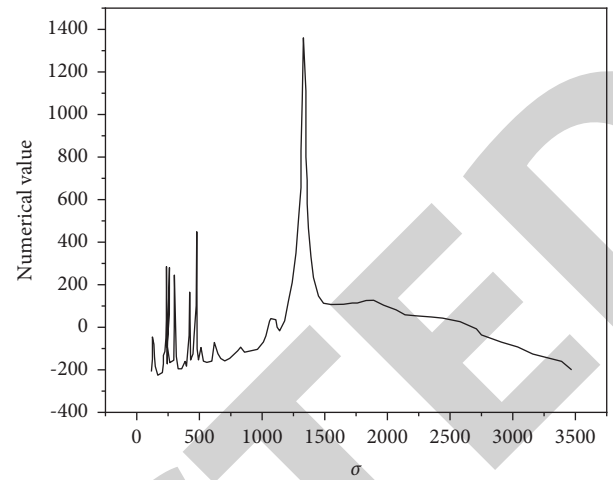

Figure 3: B-1 Raman spectra of chromogenic minerals of south red agate.

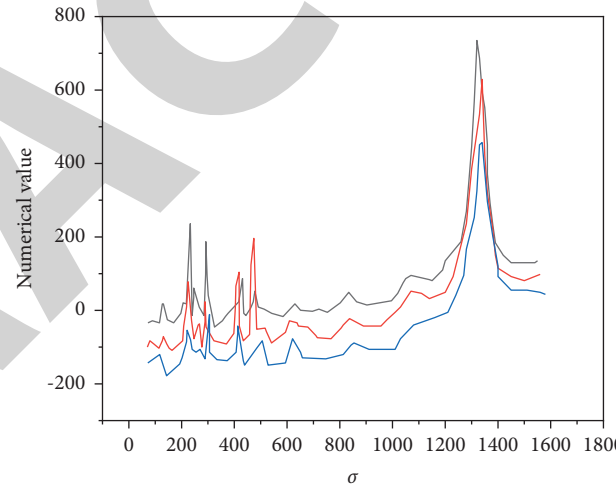

Figure 4: Raman spectra of chromogenic minerals of Nanhong agate.

mineral of south red agate and comparison samples is goethite, and there is also a very small amount of hematite. The evidence is as follows:

(1) The polarizing microscope observed that the spot-colored minerals and disseminated distribution areas of Nanhong agate are orange red. On the whole, the color tone is yellowish and translucent, which is consistent with the common color of goethite in nature.

(2) X-ray powder diffraction analysis showed that a small amount of the goethite phase was detected in central south red agate, but no obvious goethite phase was detected in yellow and colorless agate.

(3) The existence of the goethite phase was detected in the color region of dot chromogenic minerals and disseminated distribution in Raman spectroscopy.

(4) The UV-Vis absorption spectra of red and yellow samples are the superposition of typical absorption spectra of goethite and hematite.

(5) In the whole rock chemical composition analysis, the average iron content of red samples > the average iron content of yellow samples > the iron content of white comparison samples. These pieces of evidence show that red and yellow colors of Nanhong agate and the comparison sample are mainly related to the existence and content of the goethite phase, and there may be a small amount of hematite.

In addition to the content of chromogenic minerals, the color difference between goethite and hematite also affects the color of agate. When the particle size of goethite or wurtzite is 0.3~1.0 μm, the appearance is yellow, and when the particle size is 0.05~0.8 μm, the color is dark yellow. As the particle becomes smaller, the appearance color will gradually darken. When the particle size of hematite is less than 0.1 μm, the color is orange, and when the size is 0.1 ~ 0.5 μm, the color is red. When a single particle is larger than 1.5 μm, it will appear purple. When goethite and hematite are combined in a very dense way, the whole combination will appear black or dark brown. In this paper, the size of the spot-colored minerals is about 10 μm. According to the above theory, it is speculated that the appearance of agate should be opaque black. However, under the polarizing microscope, the colored minerals are translucent orange red, with fuzzy particle boundaries and no complete monocrystal characteristics. Therefore, it is speculated that the spot-colored minerals observed under the polarizing microscope are an aggregate composed of submicron goethite and a very small amount of hematite particles. In addition, there are some translucent orange red areas with disseminated distribution in Nanhong agate; no single chromogenic mineral particles can be observed, but the Raman spectrum and UV-Vis absorption spectrum show that this area is goethite with a very small amount of hematite minerals. Therefore, it is speculated that the chromogenic areas with disseminated distribution are similar to the chromogenic minerals with dot distribution, which are

an aggregate composed of submicron goethite and a small amount of hematite particles.

5. Conclusion

South red agate has a typical radial fiber structure, and there are parallel fiber crystal structures in each layer. The color of Nanhong agate in Baoshan city, Yunnan province, and Liangshan Prefecture, Sichuan province, is roughly distributed in strips, which is consistent with the distribution of nearly hexagonal reddish brown minerals. Baoshan south red agate has orange hues and developed fissures. Liangshan south red agate has rich colors and few fissures. The conventional gemmological characteristics of south red agate are similar to ordinary cryptocrystalline quartzite, but a large number of nearly red spherical inclusions are densely distributed through magnification observation. Combined with the infrared spectrum and Raman spectrum, the main mineral is α-quartz, in which the nearly hexagonal reddish brown spherical mineral inclusion is iron oxide hematite and the calcite at the crack is a mineral of late hydrothermal origin. During enlarged inspection, goethite and a small amount of hematite in Beihong agate exist in orange red punctate and disseminated forms. The size of the punctate goethite and hematite is about 10 μm, but they do not have an obvious crystal shape, and the particle boundary is fuzzy. It is speculated that it is an aggregate formed by the aggregation of submicron goethite and a small amount of hematite. The particle size of orange red goethite and hematite with disseminated distribution is not visible during magnification inspection. It is speculated that the particle size is similar to the colored minerals with dot distribution, both of which are submicron size but do not aggregate to form a dot aggregate visible under the microscope. On the whole, the content of goethite and hematite in Beihong agate is more than that in the yellow comparison sample. The higher the content of chromogenic minerals, the more red the color tone of Beihong agate. The comprehensive use of the Raman spectrum and UV-Vis absorption spectrum is of great significance for nondestructive analysis of phase composition of jewelry and jade, origin differentiation, and color classification of quartz jade.

Data Availability

The data used to support the findings of this study are available from the corresponding author upon request.

Conflicts of Interest

The authors declare that they have no conflicts of interest.

Acknowledgments

The authors are grateful to the academic funding project for Top Talents in Disciplines (Majors) of Universities in Anhui Province in 2021 (no. gxbjZD2021124) and the key project of Anhui Province Outstanding Young Talents Support Plan: Genesis of geological occurrence of southern red agate, Warring States red agate, and African red agate and significance of composition identification (no. gxyqZD2016446).

References

[1] Z. Lu, X. He, and Q. Guo, "Color and genesis of beihong agate and its spectroscopic characteristics," *Guang pu xue yu guang pu fen xi*, vol. 40, no. 8, pp. 2531–2537, 2020.

[2] K. N. Tkachenko, "Nutrition of the red fox (vulpes vulpes) in bol'shekhekhtsirskii nature reserve and its environs (southern part of the Amur river region)," *Biology Bulletin*, vol. 48, no. 8, pp. 1424–1433, 2021.

[3] A. V. Maslov, "Volcanic tuffs, red- and usual-colored clayey rocks in upper riphean–vendian deposits in the middle and southern urals: comparison of lithochemical characteristics," *Lithology and Mineral Resources*, vol. 56, no. 2, pp. 132–151, 2021.

[4] M. Redlisiak, A. Mazur, and M. Remisiewicz, "Size dimorphism and sex determination in the song thrush (turdus philomelos) migrating through the southern baltic coast," *Annales Zoologici Fennici*, vol. 57, no. 1-6, 2020.

[5] L. G. Kondratyeva, M. S. Dyachkova, and A. V. Galchenko, "The origin of genetic code and translation in the framework of current concepts on the origin of life," *Biochemistry*, vol. 87, no. 2, pp. 150–169, 2022.

[6] Y. Y. Zheng and J. Sheng, "The origin of translation," *Nature Chemistry*, vol. 13, no. 8, pp. 725-726, 2021.

[7] X. Wang, B. Li, X. Yang et al., "Characteristics of "guangyuan-wangcang" trough during late middle permian and its petroleum geological significance in northern Sichuan basin, sw China," *Petroleum Exploration and Development*, vol. 48, no. 3, pp. 655–669, 2021.

[8] T. Zhu, W. Li, Q. Wang, and Y. Hu, "Engineering geological and petrological characterization of paleoweathered rock in the k1/j2 contact zone in the ordos basin, China," *Environmental Earth Sciences*, vol. 81, no. 6, 2022.

[9] O. V. Golovanova and K. E. Pitieva, "The neopleistocene aquifer system in the region of the development of the astrakhan gas condensate field: characteristics, structures, and formation models," *Moscow University Geology Bulletin*, vol. 76, no. 6, pp. 646–655, 2022.

[10] Y. Huang, C. Tao, J. Liang et al., "Geological characteristics of the qiaoyue seamount and associated ultramafic-hosted seafloor hydrothermal system (52.1°E, southwest Indian ridge)," *Acta Oceanologica Sinica*, vol. 40, no. 11, pp. 138–146, 2022.

[11] Y. Wang, G. Zhai, G. Liu et al., "Geological characteristics of shale gas in different strata of marine facies in South China," *Journal of Earth Sciences*, vol. 32, no. 4, pp. 725–741, 2021.

[12] S. S. Krasilnikov, A. T. Basilevsky, M. A. Ivanov, and A. S. Krasilnikov, "Geological and geomorphological characteristics of high-priority landing sites for the luna-glob mission," *Solar System Research*, vol. 55, no. 2, pp. 83–96, 2021.

[13] H. J. Brink, "The variscan deformation front (VDF) in northwest Germany and its relation to a network of geological features including the Ore-Rich Harz Mountains and the European Alpine belt," *International Journal of Geosciences*, vol. 12, no. 05, pp. 447–486, 2021.

[14] E. H. Al-Khersan, S. A. Al-Taei, and A. A. Al-Zubaidi, "Marine geophysical study to explore the seafloor bathymetry and geological features at the Iraqi corridors, northwestern Arabian gulf," *Pure and Applied Geophysics*, vol. 179, no. 2, pp. 747–764, 2022.

[15] A. P. Ippolitov and D. N. Kiselev, "Geological features of the bajocian–bathonian in the reference section of the izhma river basin (European North of Russia) and the succession of ammonites of the subfamily arctocephalitinae meledina," *Stratigraphy and Geological Correlation*, vol. 29, no. 6, pp. 742–755, 2021.

[16] X. Liu, J. Liu, J. Chen, F. Zhong, and C. Ma, "Study on treatment of printing and dyeing waste gas in the atmosphere with Ce-Mn/GF catalyst," *Arabian Journal of Geosciences*, vol. 14, no. 8, 2021.

[17] S. Shriram, B. Nagaraj, S. Shankar, P. Ajay, and P. Ajay, "Deep learning-based real-time AI virtual mouse system using computer vision to avoid COVID-19 spread," *Journal of Healthcare Engineering*, vol. 2021, Article ID 8133076, 8 pages, 2021.

[18] X. Xu, L. Li, and A. Sharma, "Controlling messy errors in virtual reconstruction of random sports image capture points for complex systems," *International Journal of System Assurance Engineering and Management*, vol. 1, no. 1 2021.

[19] R. Huang, S. Zhang, W. Zhang, and X. Yang, "Progress of zinc oxide-based nanocomposites in the textile industry," *IET Collaborative Intelligent Manufacturing*, vol. 3, no. 3, pp. 281–289, 2021.